An Efficient Three-Phase Resonant DC-Link Inverter With Low Energy Consumption

Qiang Wang, Guoxian Guo, Youzheng Wang, and Jun Chen

***Abstract*—A novel three-phase resonant dc-link inverter with low energy consumption is presented to achieve efficient operation of the inverter. When the auxiliary resonant circuit is used to make the input voltage across bridge-arms become zero during every switching period, the main switching devices could achieve zero-voltage switching turn-ON and zero-current switching turn-OFF. When the metal oxide semiconductor field effect transistor (MOSFET) or the insulated gate bipolar transistor (IGBT) is used as the main switching device, the lossless switching could be completed, and the capacitive turn-ON loss caused by the internal junction capacitance of MOSFET and the turn-OFF loss caused by the tail current of IGBT are eliminated. The working process of the circuit and the realization condition of the soft-switching are analyzed. The experimental results on the three-phase prototype of 2.5 kW show that the switching devices achieve the soft-switching and the performance of the inverter is improved. Therefore, the novel topology is of great significance for improving the efficiency of the inverter.**

***Index Terms*—DC-link, inverter, resonance, zero-current switching (ZCS), zero-voltage switching (ZVS).**

I. Introduction

IN THE new development situation, the traditional hard-switching inverter has been unable to meet the needs of efficient and energy-saving production. The overlap of voltage and current of the hard-switching inverter in each switching period leads to power consumption of the switching device. Meanwhile, with the increasing of switching frequency, the switching power loss and the heating generation of the devices have increased gradually. There are higher changing rates of voltage and current in the circuit, which will produce electromagnetic interference. In modern power electronics technology, soft-switching inverters are widely used. Soft-switching inverters can achieve high frequency and soft-switching during switching, which reduces switching losses and electromagnetic interference.

Soft-switching inverters contain two categories, which are resonant pole inverters [1]–[4] and resonant dc-link inverters [5]–[21]. Wherein, resonant dc-link inverters have advantages, such as simple auxiliary circuit structure, few auxiliary devices and low hardware cost. Therefore, researchers have paid more attention to the research on resonant dc-link inverters, and have presented many resonant dc-link inverter topologies, which still need to be improved. The auxiliary circuits presented by [5]–[8] include two large-capacity energy storage capacitors between dc buses to divide the dc supply voltage, and high-frequency work of the circuit will cause changes in the neutral point potential of inverters. The auxiliary circuits presented by [9] and [10] include the clamp circuit and the steady voltage on the dc-link is higher than the dc power supply voltage, which can increase the voltage across the main switching devices, causing the decline in the reliability of the main switching devices and higher cost. The auxiliary circuits in [11]–[13] contain transformers and residual magnetic accumulation will lead to transformer saturation. The change of the neutral point potential and the saturation of the transformer will have adverse impact on the reliability of inverters. To solve the problem, it is essential to use more complicated balance control strategies of the neutral point potential and setup the demagnetization reset circuits of the transformer. The auxiliary circuits in [14]–[16] consist of three auxiliary switches, which is bad for reducing the circuit cost and simplifying the control method of the auxiliary resonant unit and will hinder miniaturization and weight reduction of the resonant dc-link inverter. The topology presented by [17] and [18] switches the bridge arm to the shoot-through state to charge the resonant inductor in each switching period, to assure that the resonant inductor has enough electric energy to make the dc-link voltage rise to the dc supply voltage, but the time when the bridge arm is in the shoot-through state needs to be accurately controlled, otherwise it will lead to the damage of dc power supply. During the work of the auxiliary units in [19] and [20], the auxiliary switches on the parallel branch must be turned ON for the charge of the resonant inductor. When the current flowing through the resonant inductor rises to the threshold value, the auxiliary switches should be turned OFF to trigger the resonant process. Thus, it is essential to supervise whether the current flowing through the resonant inductors reaches the threshold value in real time, and the threshold value changes with the load current, resulting in the complex control method of the auxiliary units. The coupled inductor in [20] and [21] is connected in series on dc buses, and the conduction loss of the coupled inductor is large, which is bad for the efficiency optimization. In addition, the switching devices in most resonant dc-link inverters could achieve zero-voltage turn-ON and zero-voltage turn-OFF. With

Manuscript received January 17, 2020; revised April 6, 2020; accepted June 2, 2020. Date of publication June 7, 2020; date of current version September 4, 2020. This work was supported in part by the Foundation of Liaoning Educational Committee under Grant L2019017, in part by the National Natural Science Foundation of China under Grant 51207069, and in part by the Scientific Research Cultivation Fund of LSHU of China under Grant 2016PY-016. Recommended for publication by Associate Editor E. Babaei. *(Corresponding author: Qiang Wang.)*

The authors are with the College of Information and Control Engineering, Liaoning Shihua University, Fushun 113001, China (e-mail: wangqiang@lnpu.edu.cn; 2907267998@qq.com; 1132333721@qq.com; 18358006251@163.com).

Color versions of one or more of the figures in this article are available online at https://ieeexplore.ieee.org.

Digital Object Identifier 10.1109/TPEL.2020.3000572

the application of three-phase inverters in the high-power situation, IGBT is often used as the switch. When IGBT switches to OFF-state, tail current will lead to turn-OFF loss. Hence, it is more meaningful to realize the zero-current turn-OFF for the inverter which takes IGBT as the switching device. However, the main switches of most resonant dc-link inverters are all connected with resonant capacitors, and the main switches and auxiliary switches on the dc bus naturally complete the zero-voltage turn-OFF when they switch to OFF-state, but they cannot achieve the zero-current turn-OFF. Besides, the above literature concerning resonant dc-link inverters does not theoretically analyze how to reduce the loss of the auxiliary circuit.

To improve performance, this article presents a new soft-switching inverter with low energy consumption, which improves the defects of the abovementioned inverters and has the following features: first, two switching devices are arranged in the auxiliary unit, without large-volume energy storage capacitors and transformers; second, compared with the more similar topology including coupled inductors presented in [20] and [21], coupled inductors in this article are in the parallel branch of dc buses and the conduction loss of the coupled inductors is much lower, which is in favor of the efficiency optimization; and third, in the control procedure of the auxiliary resonant circuit, resonance is triggered directly after the auxiliary switch ON the parallel branch is turned ON. For the control of the auxiliary switch, there is no need to monitor the change of the resonant current in real time, and the turn-ON time of the auxiliary switching device could be constant in each switching period, which facilitates the control method of the auxiliary resonant unit; fourth, the main switches of the inverter have no parallel resonant capacitors. The bus switch in series with the dc bus and the main switches can both achieve zero-voltage turn-ON and zero-current turn-OFF, which truly realizes zero loss. MOSFET and IGBT can be used as the switching devices of the presented inverter, which widens the selection range of switching devices. In this article, the working process of the inverter, including the realization conditions of the soft-switching, is analyzed at length. How to reduce the loss of the auxiliary resonant circuit is theoretically explored. Eventually, the performance of the presented three-phase inverter is verified via a 2.5-kW experimental prototype.

II. Analysis on Topology and Operating Process of the Circuit

A. Topology of the Circuit

As shown in Fig. 1, the auxiliary resonant unit contains the auxiliary switches (S_{r1} and S_{r2}), the auxiliary diodes (D_{r1} and D_{r2}), the coupled resonant inductors (L_{s1} and L_{s2}) and the resonant capacitors (C_{r1} and C_{r2}). Wherein, the number of turns of the coupled inductors L_{s1} and L_{s2} is N_1 and N_2, respectively, and the turns ratio is $n = N_2/N_1$, so the inductor value meets $L_{s2} = n^2 L_{s1}$. When the partial flux generated in $L_{s1}(L_{s2})$ is not coupled to $L_{s2}(L_{s1})$, leakage inductance will be produced and it may lead to voltage spike during turn-OFF transient of S_{r1} and S_{r2}. Therefore, L_{s1} and L_{s2} should be coupled as tightly as possible. When the auxiliary unit is in the resonant state, the main switching devices could complete zero-voltage turn-ON and zero-current turn-OFF.

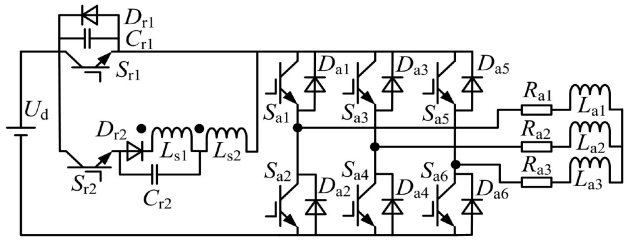

Fig. 1. Main circuit of a novel three-phase resonant dc-link inverter with low energy consumption.

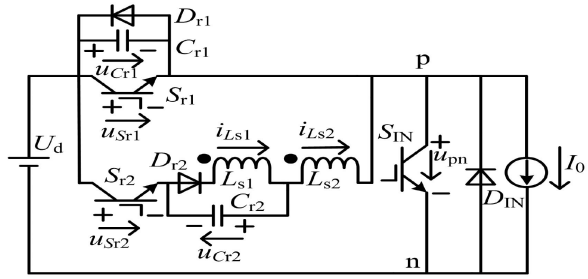

Fig. 2. Equivalent circuit of a novel three-phase resonant dc-link inverter with low energy consumption.

For simple discussion, the hypotheses are as follows:

1) each device is an ideal device;
2) the load inductor value is large enough, and I_0, the output current of the inverter, is invariant in each switching cycle, while the output load of the inverter is equivalent to the constant current source;
3) the switching device S_{IN} and the freewheeling diode D_{IN} form the equivalent circuit of the three-phase inverter;
4) leakage inductance of the coupled inductors L_{s1} and L_{s2} can be approximated as zero because L_{s1} and L_{s2} are tightly coupled.

The positive direction of the equivalent circuit and physical quantity of the inverter is shown in Fig. 2. Fig. 3 presents the theoretical waveforms of the circuit. Fig. 4 shows the equivalent circuits in every working process. The phase plane trajectory of the circuit in the switching period of one main switch is presented in Fig. 5. The special symbols in Fig. 3 are as follows: $U_1 = u_{Cr2}(t_0)$, $U_2 = u_{Cr2}(t_1)$, $U_3 = u_{Cr2}(t_6)$, $I_0 = i_{Ls2}(t_1)$, $I_1 = i_{Ls2}(t_2)$, and $nI_1 = i_{Ls1}(t_3)$.

B. Operating Process

Process 1 (t~t_0): The circuit works in a steady state and the auxiliary resonant circuit is not in the resonant condition.

Process 2 (t_0~t_1): S_{r2} switches to the conduction state at t_0, and L_{s2} slows down the variation of the current flowing through S_{r2} in order that S_{r2} achieves zero-current turn-ON. After S_{r2} switches to the conduction state, L_{s2} and C_{r2} begin to work in the resonant state. Process 2 stops when i_{Ls2} increases to I_0, u_{Cr2} decreases to U_2 and i_{Sr1} changes to zero at t_1. The motion curve trajectory of this process is shown in Fig. 5(d).

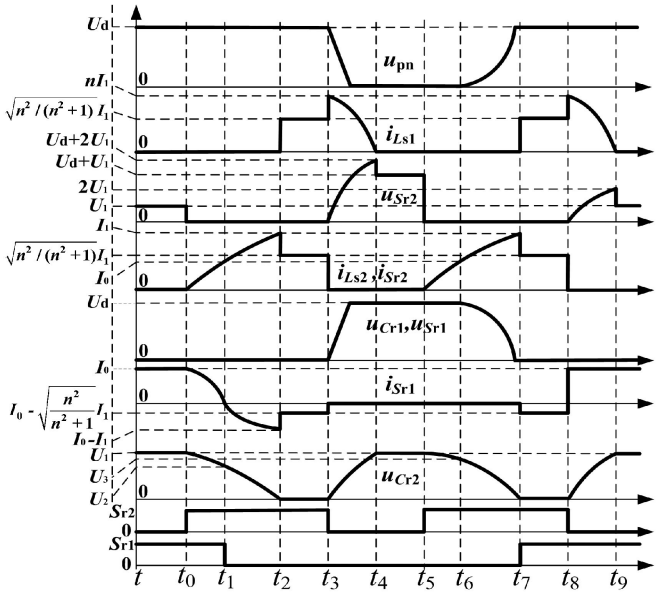

Fig. 3. Theoretical waveforms in resonant commutation.

$u_{Cr2}(t)$ and $i_{Ls2}(t)$ can be shown by the following equations:

$$u_{Cr2}(t) = U_1 \cos[\omega_1 (t - t_0)] \tag{1}$$

$$i_{Ls2}(t) = \frac{U_1}{Z_1} \sin[\omega_1 (t - t_0)] \tag{2}$$

where $\omega_1 = 1/\sqrt{L_{s2}C_{r2}}$, and $Z_1 = \sqrt{L_{s2}/C_{r2}}$.

The curvilinear motion equation of this process is presented as follows:

$$u_{Cr2}^2(t) + Z_1^2 i_{Ls2}^2(t) = U_1^2 \tag{3}$$

where $Z_1^2 = L_{s2}/C_{r2}$.

$i_{Ls2}(t_1) = I_0$ is substituted into (3), and in this process, U_2 can be obtained as follows:

$$U_2 = u_{Cr2}(t_1) = \sqrt{U_1^2 - Z_1^2 I_0^2}. \tag{4}$$

The duration of this process can be shown as

$$T_2 = t_1 - t_0 = \frac{1}{\omega_1} \arcsin\left(\frac{Z_1 I_0}{U_1}\right). \tag{5}$$

Process 3 (t_1~t_2): At t_1, S_{r1} switches to OFF-state. Because the current flowing through S_{r1} has already changed to zero before S_{r1} switches to OFF-state, S_{r1} achieves zero-current turn-OFF. After S_{r1} is turned OFF, L_{s2} and C_{r2} are still in the resonant state. C_{r2} discharges, whereas L_{s2} is charged. u_{Cr2} goes on decreasing from U_2, and i_{Ls2} goes on increasing from I_0, while the current begins to flow through D_{r1}. Process 3 stops when u_{Cr2} reduces to zero at t_2. At the same time, i_{Ls2} increases to I_1 at t_2. The motion curve trajectory of this process is shown in Fig. 5(d).

$u_{Cr2}(t)$ and $i_{Ls2}(t)$ can be shown by the following equations:

$$u_{Cr2}(t) = U_2 \cos[\omega_1 (t - t_1)] - Z_1 I_0 \sin[\omega_1 (t - t_1)] \tag{6}$$

$$i_{Ls2}(t) = \frac{U_2}{Z_1} \sin[\omega_1 (t - t_1)] + I_0 \cos[\omega_1 (t - t_1)]. \tag{7}$$

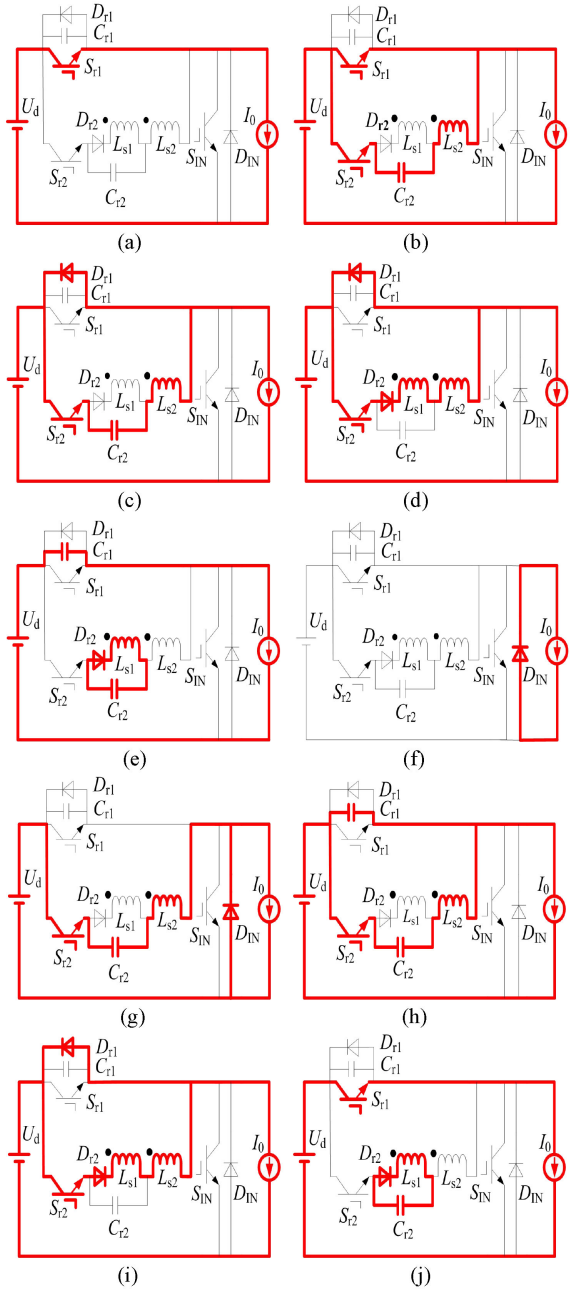

Fig. 4. Equivalent circuits in every working process. (a) Process 1. (b) Process 2. (c) Process 3. (d) Process 4. (e) Process 5. (f) Process 6. (g) Process 7. (h) Process 8. (i) Process 9. (j) Process 10.

The curvilinear motion equation of this process is presented as follows:

$$u_{Cr2}^2(t) + Z_1^2 \left[i_{Ls2}^2(t) - I_0^2\right] = U_2^2. \tag{8}$$

$u_{Cr2}(t_2) = 0$ is substituted into (8), and in this process, I_1can be obtained as follows:

$$I_1 = i_{Ls2}(t_2) = \sqrt{\frac{U_2^2}{Z_1^2} + I_0^2} = \frac{U_1}{Z_1}. \tag{9}$$

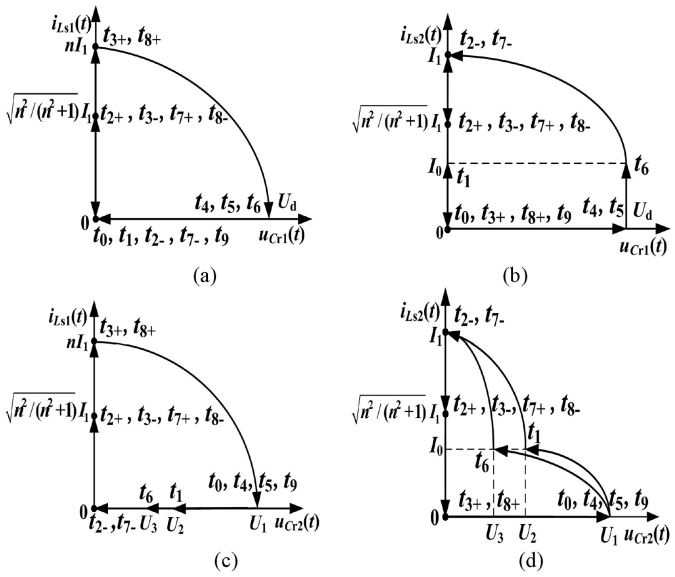

Fig. 5. Motion trajectory of the phase plane of the inverter. (a) u_{Cr1} and i_{Ls1}. (b) u_{Cr1} and i_{Ls2}. (c) u_{Cr2} and i_{Ls1}. (d) u_{Cr2} and i_{Ls2}.

The duration of this process can be shown as

$$T_3 = t_2 - t_1 = \frac{1}{\omega_1} \arctan\left(\frac{U_2}{Z_1 I_0}\right). \tag{10}$$

Process 4 (t_2∼t_3): At t_2, u_{Cr2} decreases to 0, while the current starts to flow through D_{r2}. Meanwhile, the resonant flow ends. At the end of the resonant process, the current starts to flow through L_{s1} and L_{s2} at the same time, and i_{Ls1} rapidly increases from 0 to $\sqrt{n^2/(n^2+1)}I_1$, while i_{Ls2} rapidly decreases from I_1 to $\sqrt{n^2/(n^2+1)}I_1$. Then, i_{Ls1} and i_{Ls2} remain constant.

$i_{Ls1}(t)$ and $i_{Ls2}(t)$ can be shown by the following equation:

$$i_{Ls1}(t) = i_{Ls2}(t) = \sqrt{\frac{n^2}{n^2+1}} I_1. \tag{11}$$

Process 5 (t_3∼t_4): When S_{r2} switches to OFF-state at t_3, C_{r1} and C_{r2} slow down the variation of the voltage across S_{r2} in order that S_{r2} achieves zero-voltage turn-OFF. After S_{r2} switches to OFF-state, i_{Ls1} quickly increases to nI_1, while i_{Ls2} rapidly decreases from $\sqrt{n^2/(n^2+1)}I_1$ to 0. At the same time, the load current starts to flow through C_{r1}, while L_{s1} and C_{r2} enter the resonant state. L_{s1} discharges, whereas $C_{r1}$and C_{r2} are charged. u_{Cr1} begins to linearly and positively increase from 0, and u_{Cr2} begins to nonlinearly and positively increase from 0, while i_{Ls1} goes on decreasing from nI_1. Process 5 stops when u_{Cr1} linearly increases to U_d, and u_{Cr2} increases to U_1, while i_{Ls1} is equal to zero at t_4. The motion curve trajectory of this process is shown in Fig. 5(a) and (c).

$u_{Cr1}(t)$, $u_{Cr2}(t)$, and $i_{Ls1}(t)$ can be shown by the following equations:

$$u_{Cr2}(t) = nZ_2 I_1 \sin\left[\omega_2 (t - t_3)\right] \tag{12}$$

$$i_{Ls1}(t) = nI_1 \cos\left[\omega_2 (t - t_3)\right] \tag{13}$$

$$u_{Cr1}(t) = \frac{I_0}{C_{r1}} (t - t_3) \tag{14}$$

where $\omega_2 = 1/\sqrt{L_{s1}C_{r2}}$, and $Z_2 = \sqrt{L_{s1}/C_{r2}}$.

The curvilinear motion equation of this process is presented as follows:

$$u_{Cr2}^2(t) + Z_2^2 i_{Ls1}^2(t) = n^2 Z_2^2 I_1^2 \tag{15}$$

where $Z_2^2 = L_{s1}/C_{r2}$.

$i_{Ls1}(t_4) = 0$ is substituted into (15), and in this process, U_1 can be derived as follows:

$$U_1 = nZ_2 I_1. \tag{16}$$

The duration of this process can be shown as

$$T_5 = t_4 - t_3 = \frac{\pi}{2\omega_2}. \tag{17}$$

Process 6 (t_4∼t_5): u_{pn} is kept to be zero, while I_0 continues to flow through the equivalent diode $D_{\rm IN}$. In this process, the main switch of the inverter could achieve zero-voltage turn-ON and zero-current turn-OFF.

Process 7 (t_5∼t_6): When S_{r2} switches to the conduction state at t_5, L_{s2} slows down the variation of the current flowing through S_{r2} in order that S_{r2} achieves zero-current turn-ON. After S_{r2} switches to the conduction state, L_{s2} and C_{r2} begin to work in the resonant state. Process 7 stops when u_{Cr2} changes to U_3, and i_{Ls2} is equal to I_0 at t_6. The motion curve trajectory of this process is shown in Fig. 5(b) and (d).

$u_{Cr2}(t)$ and $i_{Ls2}(t)$ can be shown by the following equations:

$$u_{Cr2}(t) = (U_d + U_1)\cos\left[\omega_1 (t - t_5)\right] - U_d \tag{18}$$

$$i_{Ls2}(t) = \frac{(U_d + U_1)}{Z_1} \sin\left[\omega_1 (t - t_5)\right]. \tag{19}$$

The curvilinear motion equation of this process is presented as follows:

$$\left[u_{Cr2}(t) + U_d\right]^2 + Z_1^2 i_{Ls2}^2(t) = (U_1 + U_d)^2 \tag{20}$$

$i_{Ls2}(t_6) = I_0$ is substituted into (20), and in this process, U_3 can be derived as follows:

$$U_3 = u_{Cr2}(t_6) = \sqrt{(U_1 + U_d)^2 - Z_1^2 I_0^2} - U_d. \tag{21}$$

The duration of this process can be shown as

$$T_7 = t_6 - t_5 = \frac{1}{\omega_1} \arcsin\left(\frac{I_0 Z_1}{U_d + U_1}\right). \tag{22}$$

Process 8 (t_6∼t_7): At t_6, L_{s2}, C_{r1}, and C_{r2} begin to work in the resonant state. u_{Cr1} begins to reduce from U_d, and u_{Cr2} goes on decreasing from U_3, while i_{Ls2} goes on increasing from I_0. Process 8 ends when u_{Cr1} and u_{Cr2} decrease to 0, while i_{Ls2} positively changes to I_1 at t_7. The motion curve trajectory of this process is shown in Fig. 5(b) and (d).

$u_{Cr1}(t)$, $u_{Cr2}(t)$, and $i_{Ls2}(t)$ can be shown by the following equations:

$$u_{Cr1}(t) = \frac{B_1}{C_{r1}\omega_3} \cos\left[\omega_3 (t - t_6)\right] - \frac{I_0 \sin\left[\omega_3 (t - t_6)\right]}{(C_{r2} + C_{r1})\omega_3} + \frac{I_0}{C_{r2} + C_{r1}} t + A_1 \tag{23}$$

$$u_{Cr2}(t) = \frac{B_1}{C_{r2}\omega_3} \cos\left[\omega_3 (t - t_6)\right] - \frac{C_{r1} I_0 \sin\left[\omega_3 (t - t_6)\right]}{C_{r2}(C_{r2} + C_{r1})\omega_3} - \frac{I_0}{C_{r2} + C_{r1}} t + B_2 \tag{24}$$

$$i_{Ls2}(t) = \frac{C_{r1}I_0}{C_{r2}+C_{r1}}\cos\left[\omega_3(t-t_6)\right] + B_1\sin\left[\omega_3(t-t_6)\right] + \frac{C_{r2}I_0}{C_{r2}+C_{r1}} \tag{25}$$

where

$$A_1 = U_d - \sqrt{\frac{C_{r2}\left(C_{r1}U_d^2 + C_{r2}U_3^2 + L_{s2}I_0^2\right)}{\left(C_{r1}+C_{r2}\right)C_{r1}}},$$

$$B_1 = \sqrt{\frac{C_{r1}U_d^2 + C_{r2}U_3^2}{L_{s2}} + I_0^2} - I_0, \omega_3 = \sqrt{\frac{C_{r1}+C_{r2}}{L_{s2}C_{r1}C_{r2}}},$$

$$B_2 = U_3 - \sqrt{\frac{C_{r1}\left(C_{r1}U_d^2 + C_{r2}U_3^2 + L_{s2}I_0^2\right)}{C_{r2}\left(C_{r1}+C_{r2}\right)}}.$$

The duration of this process can be shown as

$$T_8 = t_7 - t_6 = \frac{1}{\omega_3}\left(\arcsin\frac{C_{r2}U_3 - B_1}{\sqrt{I_0^2+B_1^2}} + \arctan\frac{B_1}{I_0}\right). \tag{26}$$

Process 9 (t_7∼t_8): At t_7, the voltage across S_{r1} has been zero. Therefore, S_{r1} achieves zero-voltage turn-ON when it switches to the conduction state at t_7, while u_{Cr2} decreases to 0, and the current starts to flow through D_{r2}. Meanwhile, the resonant process ends. At the end of the resonant process, the current starts to flow through L_{s1} and L_{s2} at the same time, and i_{Ls1} rapidly increases from 0 to $\sqrt{n^2/(n^2+1)}I_1$, while i_{Ls2} rapidly decreases from I_1 to $\sqrt{n^2/(n^2+1)}I_1$. Then, i_{Ls1} and i_{Ls2} remain constant.

$i_{Ls1}(t)$ and $i_{Ls2}(t)$ can be shown by the following equation:

$$i_{Ls1}(t) = i_{Ls2}(t) = \sqrt{\frac{n^2}{n^2+1}}I_1. \tag{27}$$

Process 10 (t_8∼t_9): When S_{r2} switches to OFF-state at t_8, C_{r2} slows down the variation of the voltage across S_{r2} in order that S_{r2} achieves zero-voltage turn-OFF. After S_{r2} switches to OFF-state, i_{Ls1} rapidly increases from $\sqrt{n^2/(n^2+1)}I_1$ to nI_1, while i_{Ls2} rapidly decreases from $\sqrt{n^2/(n^2+1)}I_1$ to 0. L_{s1} and C_{r2} begin to work in the resonant state. Process 10 stops when i_{Ls1} decreases to zero and u_{Cr2} increases to U_1. The motion curve trajectory of this process is shown in Fig. 5(c).

$u_{Cr2}(t)$ and $i_{Ls2}(t)$ can be shown by the following equations:

$$u_{Cr2}(t) = nZ_2I_1\sin\left[\omega_2(t-t_8)\right] \tag{28}$$

$$i_{Ls1}(t) = nI_1\cos\left[\omega_2(t-t_8)\right]. \tag{29}$$

The duration of this process can be shown as

$$T_{10} = \frac{\pi}{2\omega_2}. \tag{30}$$

At this point, the analysis on the operating process of the circuit in one switching period is completed.

In addition, as shown in Fig. 2, it should be noted that the black dot on the left side of the coupling inductors represents dotted terminal which shows the same polarity of voltage across coupling inductors. In Fig. 4(b), (c), (g), and (h), when C_{r2} discharges, L_{s1} and L_{s2} are not charged at the same time. The reason is that the positive polarity terminal of the voltage across C_{r2} is on the right side of C_{r2} and is not connected to two dotted terminals of the coupling inductors at the same time. If L_{s1} and L_{s2} are charged at the same time, the positive polarity terminal of the voltage across L_{s1} will be on the left side of L_{s1}, which contradicts the positive polarity terminal of the voltage across C_{r2}. In Fig. 4(e) and (j), when C_{r2} is charged, L_{s1} and L_{s2} do not discharge at the same time. The reason is that S_{r2} is in OFF-state so that no current flows through L_{s2}.

C. Design Rules

1) For zero-current turn-ON of S_{r2}, the design principle contains the following inequalities:

$$\left.\frac{di_{Sr2}(t)}{dt}\right|_{t=t_0} = \frac{U_1}{L_{s2}} \le \left(\frac{di}{dt}\right)_r \tag{31}$$

$$\left.\frac{di_{Sr2}(t)}{dt}\right|_{t=t_5} = \frac{U_d+U_1}{L_{s2}} \le \left(\frac{di}{dt}\right)_r \tag{32}$$

where $(\mathrm{d}i/\mathrm{d}t)_r$ is the permissible rising-rate of the current flowing through S_{r2}.

2) For zero-voltage turn-OFF of S_{r2}, the design principle contains the following inequalities:

$$\left.\frac{du_{Sr2}(t)}{dt}\right|_{t=t_3} = \left.\frac{2nC_{r1}I_1 + C_{r2}I_0}{C_{r1}C_{r2}}\right|_{I_0=I_{0\max}} = \left(\frac{2nU_1}{\sqrt{L_{s2}C_{r2}}} + \frac{I_{0\max}}{C_{r1}}\right) \le \left(\frac{du}{dt}\right)_r \tag{33}$$

$$\left.\frac{du_{Sr2}(t)}{dt}\right|_{t=t_8} = \left.\frac{2nI_1}{C_{r2}}\right|_{I_0=I_{0\max}} \le \left(\frac{du}{dt}\right)_r \tag{34}$$

where $(\mathrm{d}u/\mathrm{d}t)_r$ is the permissible rising-rate of the voltage across S_{r2} and $I_{0\max}$ is the maximum load current.

3) For zero-current turn-OFF of S_{r1}, it is necessary to ensure that the interval T_{d1} between the turn-ON of S_{r2} and the turn-OFF of S_{r1} is not less than the maximum value of T_2. T_{d1} can be constant, as shown in the following formula:

$$T_{d1} = \frac{\pi}{2\omega_1}. \tag{35}$$

In addition, for zero-current turn-OFF of S_{r1}, there is a need to ensure that the maximum current flowing through L_{s2} in Process 2 is no less than $I_{0\max}$. According to formula (2), the following inequality can be derived:

$$U_1 \ge Z_1I_{0\max}. \tag{36}$$

4) To guarantee that S_{r1} can realize zero-voltage turn-ON, it is requisite to ensure that the interval T_{d2} between the turn-ON of S_{r2} and turn-ON of S_{r1} is not less than the maximum value of (T_7+T_8). T_{d2} can be constant as shown in the following formula:

$$T_{d2} = \frac{\pi}{2\omega_2} + \frac{\pi}{\omega_3}. \tag{37}$$

In addition, for zero-voltage turn-ON of S_{r1}, it is also necessary to ensure that the maximum current flowing through L_{s2} in

Process 7 is no less than $I_{0\max}$. According to formula (19), the following inequality can be derived:

$$U_{\rm d} + U_1 \geq Z_1 I_{0\,\max}. \tag{38}$$

5) To simplify the control method of the auxiliary unit, the duty cycle of S_{r2} can be constant, which is shown in the following formula:

$$\rho_{Sr2} = \max\left[\frac{2\pi}{T\omega_1}, \frac{\pi}{T\omega_2} + \frac{2\pi}{T\omega_3}\right] \tag{39}$$

where *T* refers to the switching period.

6) To limit the loss of the auxiliary resonant unit, the maximum resonant current ought to satisfy the following inequality:

$$\frac{U_1}{Z_1} < 2I_{0\max}. \tag{40}$$

7) To guarantee that u_{pn} rises and drops within T_V, the design principle contains the following inequalities:

$$C_{r1}U_d/I_{0\min} \leq T_V \tag{41}$$

$$\pi/\omega_3 \leq T_V \tag{42}$$

where $I_{0\min}$ denotes the minimum value of the load current during the operation of auxiliary circuits.

8) The turns ratio *n* should satisfy the following inequalities to achieve soft-switching.

According to the inequalities (31)–(34), (36), and (38), the limitation for the turns ratio *n* can be, respectively, derived

$$n \geq \sqrt{\frac{U_1}{L_{s1}\,(di/dt)_{\,r}}} \tag{43}$$

$$n \geq \sqrt{\frac{U_d + U_1}{L_{s1}\,(di/dt)_{\,r}}} \tag{44}$$

$$n \leq \frac{[(du/dt)_{\,r} - (I_{0\max}/C_{r1})]\,C_{r2}}{2I_1} \tag{45}$$

$$n \leq \frac{(du/dt)_{\,r}C_{r2}}{2I_1} \tag{46}$$

$$n \leq \frac{U_1}{I_{0\max}\sqrt{L_{s1}/C_{r2}}} \tag{47}$$

$$n \leq \frac{U_d + U_1}{I_{0\max}\sqrt{L_{s1}/C_{r2}}}. \tag{48}$$

D. Maximum Voltage and Current of the Devices in the Circuit

In Process 5, the voltage u_{Cr1} of C_{r1} reaches the maximum value U_d; the voltage u_{Sr1} of S_{r1} reaches the maximum value U_d; the voltage u_{Sr2} of S_{r2} reaches the maximum value $(U_d + 2U_1)$; and D_{r1} bears the maximum voltage U_d. In Process 7, D_{r2} withstands the maximum voltage $(U_d + 2U_1)$. At the end of Process 10, when i_{Ls1} decreases to zero, the voltage u_{Cr2} of C_{r2} reaches the maximum value U_1.

The maximum value of the current flowing through D_{r1} can be presented as follows:

$$I_{Dr1\max} = \sqrt{\frac{n^2}{n^2+1}}\frac{U_1}{Z_1}. \tag{49}$$

The maximum values of the current flowing through C_{r2}, L_{s1}, L_{s2}, D_{r2}, and S_{r2} can be presented as follows:

$$I_{Cr2\max} = I_{Ls1\max} = I_{Ls2\max} = I_{Dr2\max} = I_{Sr2\max} = \frac{U_1}{Z_1}. \tag{50}$$

The positive and negative maximum values of the current flowing through S_{r1} can be respectively presented as follows:

$$I_{Sr1\max(+)} = I_{0\max} \tag{51}$$

$$I_{Sr1\max(-)} = I_{0\max} - \frac{U_1}{Z_1}. \tag{52}$$

III. Explanations on the Required Soft-Switching Conditions

1) S_{r2} achieves zero-current turn-ON on condition that the rising-rate of the current flowing through S_{r2} during turn-ON transient is no more than the set value. The turn-ON loss of S_{r2} is reduced by limiting the rising-rate of the current at the instant of turn-ON. L_{s2} can slows down the variation of the current flowing through S_{r2}. As shown in Fig. 4(b) and (g), the rising-rate of the current flowing through L_{s2} is equal to the rising-rate of the current flowing through S_{r2} during turn-ON transient. Based on the above explanation, the inequalities (31) and (32) can be derived.
2) S_{r2} achieves zero-voltage turn-OFF on condition that the rising-rate of the voltage across S_{r2} during turn-OFF transient is no more than the set value. The turn-OFF loss of S_{r2} is reduced by limiting the rising-rate of the voltage at the instant of turn-OFF. C_{r1} and C_{r2} can slow down the variation of the voltage across S_{r2}. As shown in Fig. 4(e) and (j), the rising-rate of the voltage across C_{r1} and C_{r2} is equal to the rising-rate of the voltage across S_{r2} during turn-OFF transient. Based on the above explanation, the inequalities (33) and (34) can be derived.
3) S_{r1} achieves zero-voltage turn-ON on condition that the voltage across S_{r1} has been equal to zero before S_{r1} is turned ON. As shown in Fig. 4(g) and (h), after S_{r2} is turned ON, L_{s2}, C_{r1}, and C_{r2} are in the resonant state. The voltage across S_{r1} will reduce to zero when Process 8 ends. When S_{r1} is turned ON in Process 9, S_{r1} will achieve zero-voltage turn-ON. For zero-voltage turn-ON of S_{r1} in full load range, it is required that the interval time between the turn-ON of S_{r2} and turn-ON of S_{r1} is not less than the maximum duration of Process 7 and 8. Based on the above explanation, the formula (37) can be derived. In addition, it can be seen from Fig. 4(g) that the maximum current flowing through L_{s2} in Process 7 should be no less than $I_{0\max}$ to make the operation of the auxiliary circuit enter Process 8 for zero-voltage turn-ON of S_{r1} in full load range. Therefore, the formula (38) can be derived.

4) S_{r1} achieves zero-current turn-OFF on condition that the current flowing through S_{r1} has been equal to zero before S_{r1} is turned OFF. As shown in Fig. 4(b), after S_{r2} is turned ON, L_{s2} and C_{r2} are in the resonant state. The current flowing through S_{r1} will reduce to zero when Process 2 ends. When S_{r1} is turned OFF in Process 3, S_{r1} will achieve zero-current turn-OFF. For zero-current turn-OFF of S_{r1} in full load range, it is required that the interval time between the turn-ON of S_{r2} and turn-OFF of S_{r1} should be no less than the maximum duration of Process 2. Based on the above explanation, the formula in (35) can be derived. In addition, it can be seen from Fig. 4(b) that the maximum current flowing through L_{s2} in Process 2 should be no less than $I_{0\max}$ to make the operation of the auxiliary circuit enter Process 3 for zero-voltage turn-OFF of S_{r1} in full load range. Therefore, the formula in (36) can be derived.
5) Main switching devices achieve zero-voltage turn-ON and zero-current turn-OFF on the condition that the voltage across bridge-arm has reduced to zero in a short time before main switching devices act. For zero-voltage turn-ON and zero-current turn-OFF of main switching devices in full load range, it is required that the maximum time when the voltage across bridge-arm drops from dc power supply to zero should be no more than the set time. Based on the above explanation, the formula (41) can be derived.

IV. Analysis on the Loss of the Auxiliary Circuits

Because S_{r1} and S_{r2} achieve soft-switching, the switching loss of S_{r1} and S_{r2} is eliminated. S_{r1}, S_{r2}, D_{r1}, and D_{r2} have conduction loss. L_{s1}, L_{s2}, C_{r1}, and C_{r2} have loss in the internal resistance. V_{CE} indicates ON-state voltage across switches; V_{EC} indicates ON-state voltage across diodes; f_c indicates switching frequency. The inherent resistance of L_{s1}、L_{s2}、C_{r1}, and C_{r2} is set as R_{Ls1}、R_{Ls2}、R_{Cr1}, and R_{Cr2}, respectively.

The loss of S_{r1} and S_{r2} is as follows:

$$P_{S_{r1}} = V_{CE}\left[\int_{t_0}^{t_1}\left(I_0 - i_{Ls2}(t)\right)dt + \int_{t_8}^{t_9} I_0 dt\right] f_c = V_{CE}\left[\frac{I_0\pi}{2\omega_2} + \frac{I_0}{\omega_1}\arcsin\left(\frac{Z_1 I_0}{U_1}\right) + \frac{U_1}{Z_1\omega_1}\sqrt{1-\left(\frac{Z_1 I_0}{U_1}\right)^2}\right] f_c \tag{53}$$

$$P_{S_{r2}} = V_{CE}\begin{bmatrix}\int_{t_0}^{t_1} i_{Ls2}(t)dt + \int_{t_1}^{t_2} i_{Ls2}(t)dt + \int_{t_2}^{t_3} i_{Ls2}(t)dt \\ +\int_{t_5}^{t_6} i_{Ls2}(t)dt + \int_{t_6}^{t_7} i_{Ls2}(t)dt + \int_{t_7}^{t_8} i_{Ls2}(t)dt\end{bmatrix} f_c = V_{CE}\begin{bmatrix}\frac{U_2 I_0/(Z_1 I_0)}{\omega_1\sqrt{1+(U_2/Z_1 I_0)^2}} + \frac{C_{r1} I_0 \sin(\omega_3 T_8)}{C_{r1}+C_{r2}} + \frac{B_1}{\omega_3} \\ +\frac{U_2}{Z_1\omega_1}\left(1 - \frac{1}{\sqrt{1+(U_2/(Z_1 I_0))^2}}\right) + \frac{C_{r2} I_0 T_8}{C_{r1}+C_{r2}} \\ \frac{U_d+U_1}{Z_1\omega_1}\left(1-\left(\frac{I_0 Z_2}{U_d+U_1}\right)^2\right) - \frac{B_1}{\omega_3}\cos(\omega_3 T_8)\end{bmatrix} f_c. \tag{54}$$

The loss of D_{r1} and D_{r2} is as follows:

$$P_{D_{r1}} = V_{EC}\begin{bmatrix}\int_{t_1}^{t_2}\left(i_{Ls2}(t) - I_0\right)dt + \int_{t_2}^{t_3}\left(\sqrt{\frac{n^2}{n^2+1}} I_1 - I_0\right)dt \\ +\int_{t_7}^{t_8}\left(\sqrt{\frac{n^2}{n^2+1}} I_1 - I_0\right)dt\end{bmatrix} f_c = V_{EC}\begin{bmatrix}\frac{I_0}{\omega_1}\left(\frac{U_2/(Z_1 I_0)}{\sqrt{1+(U_2/(Z_1 I_0))^2}} - \arctan\left(\frac{U_2}{Z_1 I_0}\right)\right) \\ +\frac{U_2}{Z_1\omega_1}\left(1 - \frac{1}{\sqrt{1+(U_2/(Z_1 I_0))^2}}\right)\end{bmatrix} f_c \tag{55}$$

$$P_{D_{r2}} = V_{EC}\begin{bmatrix}\int_{t_2}^{t_3} i_{Ls1}(t)dt + \int_{t_3}^{t_4} i_{Ls1}(t)dt \\ +\int_{t_7}^{t_8} i_{Ls1}(t)dt + \int_{t_8}^{t_9} i_{Ls1}(t)dt\end{bmatrix} f_c = V_{EC}\left[\frac{nI_1}{\omega_2} + \frac{nI_1}{\omega_3}\right] f_c. \tag{56}$$

The loss of L_{s1} and L_{s2} is as follows:

$$P_{Ls1} = f_c\begin{bmatrix}\int_{t_2}^{t_3} i_{Ls1}^2(t)dt + \int_{t_3}^{t_4} i_{Ls1}^2(t)dt \\ +\int_{t_7}^{t_8} i_{Ls1}^2(t)dt + \int_{t_8}^{t_9} i_{Ls1}^2(t)dt\end{bmatrix} R_{Ls1} = f_c\left[\frac{n^2 I_1^2(2\pi+1)}{4\omega_2} + \frac{n^2 I_1^2(2\pi+1)}{4\omega_3}\right] R_{Ls1}. \tag{57}$$

$$P_{Ls2} = f_c\begin{bmatrix}\int_{t_0}^{t_1} i_{Ls2}^2(t)dt + \int_{t_1}^{t_2} i_{Ls2}^2(t)dt + \int_{t_2}^{t_3} i_{Ls2}^2(t)dt \\ +\int_{t_5}^{t_6} i_{Ls2}^2 dt + \int_{t_6}^{t_7} i_{Ls2}^2(t)dt + \int_{t_7}^{t_8} i_{Ls2}^2(t)dt\end{bmatrix} R_{Ls2} = f_c\begin{bmatrix}\frac{U_1^2\arcsin\left(\frac{Z_1 I_0}{U_1}\right)}{2Z_1^2\omega_1} - \frac{U_1^2\sin\left(2\arcsin\left(\frac{Z_1 I_0}{U_1}\right)\right)}{4Z_1^2} \\ +\frac{U_2^2\arctan(U_2/(Z_1 I_0))}{2Z_1^2\omega_1} - \frac{U_2^3/(Z_1 I_0)}{4Z_1^2\sqrt{1+(U_2/(Z_1 I_0))^2}} \\ +\frac{(I_0 U_2/Z_1)}{\omega_1\sqrt{1+(U_2/(Z_1 I_0))^2}} + \frac{C_{r2}^2 I_0^2(2T_8+\sin(\omega_3 T_8))}{4(C_{r1}+C_{r2})^2}\end{bmatrix} R_{Ls2}. \tag{58}$$

The loss of C_{r1} and C_{r2} is as follows:

$$P_{Cr1} = f_c\left[\int_{t_3}^{t_4} I_0^2 dt + \int_{t_6}^{t_7}\left(i_{Ls2}(t) - I_0\right)^2 dt\right] R_{Cr1} = f_c\begin{bmatrix}\frac{C_{r2}^2 I_0^2(2T_8+\sin(\omega_3 T_8))}{4(C_{r1}+C_{r2})^2} + \frac{C_{r1}^2 I_0^2 T_8^2}{(C_{r1}+C_{r2})^2} \\ +\frac{I_0^2\pi}{2\omega_3} + \frac{B_1^2 T_8}{2\omega_3} - \frac{B_1^2\sin(\omega_3 T_8)}{2\omega_3}\end{bmatrix} R_{Cr1} \tag{59}$$

$$P_{Cr2} = f_c\begin{bmatrix}\int_{t_0}^{t_1} i_{Ls2}^2(t)dt + \int_{t_1}^{t_2} i_{Ls2}^2(t)dt + \int_{t_3}^{t_4} i_{Ls1}^2(t)dt \\ +\int_{t_5}^{t_6} i_{Ls2}^2(t)dt + \int_{t_6}^{t_7} i_{Ls2}^2(t)dt + \int_{t_8}^{t_9} i_{Ls1}^2(t)dt\end{bmatrix} R_{Cr2} = f_c\begin{bmatrix}\frac{U_2^2\arctan\left(\frac{U_2}{Z_1 I_0}\right)}{2Z_1^2\omega_1} - \frac{U_1^2\sin\left(2\arcsin\left(\frac{Z_1 I_0}{U_1}\right)\right)}{4Z_1^2} \\ +\frac{U_1^2\arcsin\left(\frac{Z_1 I_0}{U_1}\right)}{2Z_1^2\omega_1} - \frac{U_2^3/(Z_1 I_0)}{4Z_1^2\sqrt{1+(U_2/Z_1 I_0)^2}} + \\ \frac{C_{r2}^2 I_0^2(T_8+\sin(\omega_3 T_8))}{4(C_{r1}+C_{r2})^2} + \frac{2I_1^2 n^2(2\pi+1)}{4\omega_2}\end{bmatrix} R_{Cr2}. \tag{60}$$

I_0 in the above calculation expression is taken in accordance with the effective value of the load current.

$P_{\rm add}$, the overall loss of the auxiliary circuit, is as follows:

$$P_{\rm add} = P_{Sr1} + P_{Sr2} + P_{Dr1} + P_{Dr2} + P_{Ls1} + P_{Ls2} + P_{Cr1} + P_{Cr2}. \quad (61)$$

The expression of the overall loss of the auxiliary circuit is used to obtain the partial derivatives of L_{s1}, L_{s2}, C_{r1}, and C_{r2}, respectively. By judging the relationship between the partial derivative and zero, the influence of the resonant parameter changes on the auxiliary circuit loss is analyzed.

The expression of partial derivative with respect to L_{s1} is as follows:

$$\frac{\partial P_{\rm add}}{\partial L_{s1}} = V_{CE}\left[\frac{C_{r2}I_0 \arcsin\frac{Z_1 I_0}{U_1}}{2\sqrt{L_{s2}C_{r2}}} + \frac{nI_1\left(C_{r1}+C_{r2}\right)}{8L_{s2}C_{r1}C_{r2}} + \frac{n^2 I_1^2(2\pi+1)}{8\sqrt{L_{s2}C_{r2}}} - \frac{I_0^2 Z_2}{C_{r2}^2\left(U_d+U_1\right)^2}\right] f_c + V_{EC}\left[\frac{nI_1 C_{r2}}{2\sqrt{L_{s2}C_{r2}}}\right] f_c + f_c\left[\frac{n^2 I_1^2(2\pi+1)C_{r2}}{8\sqrt{L_{s2}C_{r2}}}\right] R_{Ls1} + f_c\left[\frac{nI_1 C_{r2}}{2\sqrt{L_{s2}C_{r2}}}\right] R_{Cr1} + f_c\left[\frac{I_0^2}{2C_{r2}^2 U_1\sqrt{1-\left(\frac{Z_1 I_0}{U_1}\right)^2}} + \frac{I_0 C_{r2}\omega_1 U_2/(Z_1 I_0)}{2\sqrt{1+\left(\frac{U_2}{Z_1 I_0}\right)^2}}\right] R_{Ls2} f_c\left[\frac{B_1 \sin\left(\omega_3 T_8\right)}{\omega_3} + \frac{n^2 I_0^2(2\pi+1)}{8}\right] R_{Cr2} > 0. \quad (62)$$

The expression of partial derivative with respect to L_{s2} is as follows:

$$\frac{\partial P_{add}}{\partial L_{s2}} = V_{CE}\left[\frac{I_0^2}{2C_{r2}^2 U_1\sqrt{1-\left(\frac{Z_1 I_0}{U_1}\right)^2}} - \frac{2I_0^2 Z_2}{C_{r2}\left(U_d+U_1\right)^2}\right] f_c + V_{EC}\left[\frac{2U_2 L_{s2}}{C_{r2}\sqrt{1+\left(\frac{U_2 C_{r2}}{L_{s2} I_0}\right)^2}} + \frac{nI_1\left(C_{r1}+C_{r2}\right)}{2L_{s2}C_{r1}C_{r2}}\right] f_c + f_c\left[\frac{n^2 I_1^2\left(2\pi+1\right)}{8L_{s2}C_{r2}} + \frac{nI_1\left(C_{r1}+C_{r2}\right)}{8L_{s2}C_{r1}C_{r2}}\right] R_{Ls1} + f_c\left[\frac{I_0^2}{A_2^2}\left(\arcsin\frac{C_{r2}U_3 - B_1}{\sqrt{I_0^2+B_1^2}} + \arctan\frac{B_1}{I_0}\right)\right] R_{Ls2} + f_c\left[\frac{U_2}{Z_1\omega_1}\frac{Z_1^2 I_0^2}{Z_1^2 I_0^2 + U_2^2} - \frac{n^2 I_1^2(2\pi+1)C_{r2}}{8\sqrt{L_{s2}C_{r2}}}\right] R_{Cr1} + f_c\left[I_0^2\left(2\arctan\frac{U_2}{Z_1 I_0} + \frac{U_2 Z_1 I_0}{Z_1^2 I_0^2 + U_2^2}\right)\right] R_{Cr2} > 0. \quad (63)$$

It is indicated from (62)–(65) that with the increase of L_{s1}, L_{s2}, C_{r1}, and C_{r2}, the loss of the auxiliary circuit will increase, and thus there is a need to try to take the minimum value of L_{s1}, L_{s2}, C_{r1}, and C_{r2} on the premise of satisfying design rules.

V. Parametric Design

The voltage across the dc power supply $U_d = 250$ V, the maximum load current $I_{0\max} = 15$ A, the minimum load current during the operation of the auxiliary circuit $I_{0\min} = 2$ A, the allowable changing rate of the voltage across switching devices $(\mathrm{d}u/\mathrm{d}t)_r = 600$ V/μs, the allowable changing rate of the current flowing through switching devices $(\mathrm{d}i/\mathrm{d}t)_r = 55$A/$\mu$s, the maximum rising and dropping time for dc bus voltage at each switching period $T_V = 4.9$ μs, the switching frequency $f_c = 20$ kHz, and the switching period $T = 50$ μs.

The expression of partial derivative with respect to C_{r1} is as follows:

$$\frac{\partial P_{\rm add}}{\partial C_{r1}} = V_{CE}\left[\frac{I_0 \sin\left(\omega_3 T_8\right) - C_{r1} I_0 \sin\left(\omega_3 T_8\right)}{\left(C_{r1}+C_{r2}\right)^2} + \frac{\omega_3 T_8 - \frac{T_8}{\omega_3^2}}{\omega_3^2} + \frac{\left(U_d+U_1\right) B_1 \cos\left(\omega_3 T_8\right)}{2Z_1\omega_1\omega_3^2}\right] f_c + V_{EC}\left[\frac{nI_1\left(L_{s2}C_{r2}\left(C_{r1}+C_{r2}\right) - L_{s2}C_{r1}C_{r2}\right)}{2\left(C_{r1}+C_{r2}\right)^2\omega_3}\right] f_c + f_c \times \left[\frac{n^2 I_1^2(2\pi+1)\left(L_{s2}C_{r2}\left(C_{r1}+C_{r2}\right) - L_{s2}C_{r1}C_{r2}\right)}{8\left(C_{r1}+C_{r2}\right)^2\omega_3}\right] R_{Ls1} + f_c\left[\frac{\left(U_d+U_1\right)\sin\left(\omega_3 T_8\right)}{Z_1\omega_1}\right] R_{Ls2} + f_c\left[\frac{I_0 T_8 - I_0 T_8 C_{r2}}{\left(C_{r1}+C_{r2}\right)}\right] R_{Cr1} f_c\left[\frac{B_1\omega_3 \sin\left(\omega_3 T_8\right)}{\omega_3^2} + \frac{I_0^2 \sin\left(\omega_3 T_8\right)}{\left(C_{r1}+C_{r2}\right)^2}\right] R_{Cr2} > 0. \quad (64)$$

The expression of partial derivative with respect to C_{r2} is as follows:

$$\frac{\partial P_{add}}{\partial C_{r2}} = V_{CE}\left[\frac{I_0\pi L_{s1}}{4\sqrt{L_{s1}C_{r2}}} + \frac{I_0 L_{s2}}{2\sqrt{L_{s2}C_{r2}}}\arcsin\frac{Z_1 I_0}{U_1} - \frac{U_1\sqrt{1-\left(\frac{Z_1 I_0}{U_1}\right)^2}}{C_{r2}^2}\right] f_c + V_{EC}\left[\frac{I_0\sqrt{L_{s2}C_{r2}}}{1+\frac{C_{r2}U_2^2}{L_{s2}I_0^2}} + \frac{nI_1}{2L_{s1}C_{r2}}\right] f_c + f_c\left[\frac{n^2 I_1^2(2\pi+1)C_{r2}}{8L_{s2}C_{r2}} + \frac{n^2 I_1^2(2\pi+1)}{8}\right] R_{Ls1} + f_c\left[\frac{2U_2 L_{s2}C_{r2}I_0^2 + 3U_2^2 C_{r2}^2}{L_{s2}C_{r2}^2 I_0^2 + U_2^2 C_{r2}^3} - \frac{2I_0^2 Z_2}{C_{r2}\left(U_1+U_d\right)^2}\right] R_{Ls2} + f_c\left[\frac{nI_1\left(L_{s2}C_{r2}\left(C_{r1}+C_{r2}\right) - L_{s2}C_{r1}C_{r2}\right)}{2\left(C_{r1}+C_{r2}\right)^2\omega_3}\right] R_{Cr1} f_c\left[\frac{n^2 I_0^2(2\pi+1)}{8} + \frac{L_{s2}I_0}{C_{r2}^2 U_1}\right] R_{Cr2} > 0.t \quad (65)$$

The specific design process is as follows.

1) In order to simplify the parameter design process and meet the requirement that the maximum voltage of S_{r2} is not

greater than $2U_d$, the following formula must be satisfied.

$$U_1 = \frac{U_d}{2} = 125 \text{ V}. \tag{66}$$

2) In order to achieve zero-current turn-ON of S_{r2} in the full load range, the following inequalities can be obtained from (31) and (32)

$$L_{s2} \geq \frac{U_1}{\left(\frac{di}{dt}\right)_r} = 2.27\ \mu\text{H} \tag{67}$$

$$L_{s2} \geq \frac{U_d + U_1}{\left(\frac{di}{dt}\right)_r} = 6.82\ \mu\text{H}. \tag{68}$$

In summary, the value range of L_{s2} is $L_{s2} \geq 6.82\,\mu$H. According to the changing relationship between L_{s2} and auxiliary circuit loss obtained from analysis on the loss of the auxiliary circuit in Section IV, $L_{s2} = 6.82\ \mu$H should be taken theoretically, but $L_{s2} = 7\ \mu$H is taken actually, when manufacturing tolerances of L_{s2} and the influence of temperature change on L_{s2} are taken into account.

3) In order to achieve zero-current turn-OFF of S_{r2} in the full load range, according to (36), the following inequality can be obtained as follows:

$$\frac{Z_1 I_{0\max}}{U_1} = \frac{\sqrt{L_{s2}/C_{r2}}I_{0\max}}{U_1} \leq 1. \tag{69}$$

$U_1 = 125$ V, $L_{s2} = 7\ \mu$H, and $I_{0\max} = 15$ A are substituted into formula (69), and the following inequality can be obtained as follows:

$$C_{r2} \geq 0.1\ \mu\text{F}. \tag{70}$$

According to the changing relationship between C_{r2} and auxiliary circuit loss obtained from analysis on the loss of the auxiliary circuit in Section IV, $C_{r2} = 0.1\ \mu$F should be taken theoretically, but $C_{r2} = 0.22\ \mu$F is taken actually, when manufacturing tolerances of C_{r2} and the influence of temperature change on C_{r2} are considered.

4) In order to achieve zero-voltage turn-OFF of S_{r2} in the full load range, $U_1 = 125$ V, $L_{s2} = 7\ \mu$H, $C_{r2} = 0.22\ \mu$F, and $(du/dt)_r = 600$ V/μs are substituted into formula (46), and the following inequality can be obtained as follows:

$$n \leq 2.95. \tag{71}$$

To simplify calculation, $n = 1$ is taken, namely $L_{s1} = L_{s2} = 7\ \mu$H.

$n = 1$, $U_1 = 125$ V, $L_{s2} = 7\ \mu$H, $C_{r2} = 0.22\ \mu$F, and $(\mathrm{d}u/\mathrm{d}t)_r = 600\,\text{V}/\mu\text{s}$ are substituted into formula (33), and the following inequality can be obtained as follows:

$$C_{r1} \geq 0.0377\ \mu\text{F}. \tag{72}$$

According to the changing relationship between C_{r1} and auxiliary circuit loss obtained from analysis on the loss of the auxiliary circuit in Section IV, $C_{r1} = 0.0377\ \mu$F should be taken theoretically, but $C_{r1} = 0.039\ \mu\text{F} = 39$ nF is taken actually, when manufacturing tolerances of C_{r1} and the influence of temperature change on C_{r1} are taken into account.

5) $U_1 = 125$ V, $I_{0\max} = 15$ A, $C_{r1} = 39$ nF, $C_{r2} = 0.22\ \mu$F, $L_{s2} = 7\ \mu$H, and $n = 1$ are substituted into (34), and the following inequality can be obtained as follows:

$$\left.\frac{du_{Sr2}(t)}{dt}\right|_{t=t_8} = \left.\frac{2I_1}{C_{r2}}\right|_{I_0=I_{0\max}} = 201.8\ \text{V}/\mu\text{s} < \left(\frac{du}{dt}\right)_r. \tag{73}$$

Therefore, the parameter design meets the condition that S_{r2} can realize zero-voltage turn-OFF in the full load range.

6) $L_{s2} = 7\ \mu$H and $C_{r2} = 0.22\ \mu$F are substituted into (35), and the following formula can be obtained as follows:

$$T_{d1} = \frac{\pi}{2\omega_1} = 1.9\ \mu\text{s}. \tag{74}$$

Therefore, S_{r1} can achieve zero-current turn-OFF in the full load range on conduction that T_{d1} is equal to 1.9 μs.

7) $L_{s1} = L_{s2} = 7\ \mu$H, $C_{r1} = 39$ nF, and $C_{r2} = 0.22\ \mu$F are substituted into (37), and the following formula can be obtained as follows:

$$T_{d2} = \frac{\pi}{2\omega_2} + \frac{\pi}{\omega_3} = 3.4\ \mu\text{s}. \tag{75}$$

Therefore, S_{r1} can achieve zero-voltage turn-ON in the full load range on conduction that T_{d2} is equal to 3.4 μs.

8) $L_{s1} = L_{s2} = 7\ \mu$H,$C_{r1} = 39$ nF, and $C_{r2} = 0.22\ \mu$F are substituted into (39), and the following formula can be obtained as follows:

$$\rho_{Sr2} = \max\left[\frac{2\pi}{T\omega_1}, \frac{\pi}{T\omega_2} + \frac{2\pi}{T\omega_3}\right] = 0.155. \tag{76}$$

Hence, the parameter design meets the condition for simplifying the control of the auxiliary circuit in the full load range.

9) $U_1 = 125$ V, $L_{s1} = L_{s2} = 7\ \mu$H, $I_{0\,\max} = 15$ A, $C_{r1} = 39$ nF, and $C_{r2} = 0.22\ \mu$F are substituted into (40), and the following inequality can be obtained as follows:

$$\frac{U_1}{Z_1} = 22.2A < 30A. \tag{77}$$

Therefore, the parameter design meets the limiting condition of the maximum resonant current in the full load range.

10) $C_{r1} = 39$ nF, $C_{r2} = 0.22\ \mu$F, $L_{s1} = L_{s2} = 7\ \mu$H, $T_V = 4.9\ \mu$s, $U_d = 250$ V, and $I_{0\,\min} = 2$ A are substituted into (41) and (42), and the following inequalities can be obtained as follows:

$$C_{r1}U_d/I_{0\min} = 4.88\ \mu\text{s} < 4.9\ \mu\text{s} \tag{78}$$

$$\pi/\omega_3 = 1.51\ \mu\text{s} < 4.9\ \mu\text{s}. \tag{79}$$

Thus, the parameter design meets the condition that the dc bus voltage can rise and drop within $T_V = 4.9\,\mu$s in each switching period.

11) $U_d = 250$ V, $U_1 = 125$ V, $L_{s1} = L_{s2} = 7\ \mu$H, $C_{r1} = 0.039\ \mu$F, $C_{r2} = 0.22\ \mu$F, $(du/dt)_r = 600$ V/μ, $(di/dt)_r = 55$ A/μs, and $\mathrm{I0}_{\max} = 15$ A are substituted into (43)–(48). The following inequalities can be obtained as follows:

$$0.99 \leq n \leq 1.07. \tag{80}$$

Therefore, $n = 1$ meets the conditions of soft-switching.

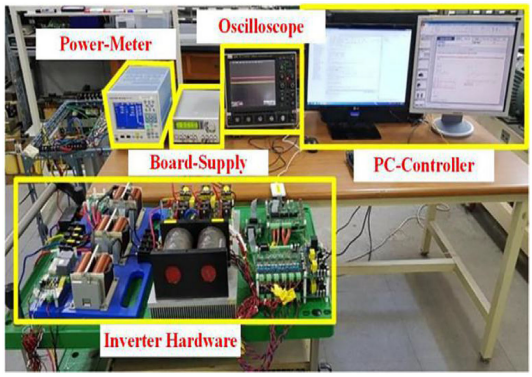

Fig. 6. Photograph of the experimental platform.

TABLE I
PARAMETERS AND COMPONENTS OF THE PROTOTYPE

Components	Parameters
Control board	DSP TMS320F2812
Driving chip	EXB841
Rated output power	2.5kW
DC power supply (U_d)	250V
Maximum load current (I_{0max})	15A
Minimum load current during the operation of auxiliary circuits (I_{0min})	2A
Switching frequency (f_c)	20kHz
Output frequency (f_0)	50Hz
The duty cycle of trigger pulse of the auxiliary switch S_{r2}	0.155
S_{r1} and S_{a1}~S_{a6}	1MBH25D-120 (1200V,25A)
S_{r2}	1MBH60-100 (1000V,60A)
D_{r2}	RHRG50120 (1200V,50A)
C_{r1}	39nF
C_{r2}	0.22μF
$L_{s1}$and L_{s2}	7μH
The turns ratio n	1
Load inductor L_{a1}, L_{a2} and L_{a3}	1mH
Load resistance R_{a1}, R_{a2} and R_{a3}	7.5Ω

12) Based on the above parameters, the range of the voltage across C_{r1} is from 0 to 250 V; the range of the voltage across C_{r2} is from 0 to 125 V; the range of the current flowing through L_{s1} and L_{s2} is from 0 to 22.2 A; the range of the voltage across S_{r1} is from 0 to 250 V; the range of the voltage across S_{r2} and D_{r2} is from 0 to 500 V; the range of the current flowing through S_{r1} is from 0 to 15 A; and the range of the current flowing through S_{r2} and D_{r2} is from 0 to 22.2 A. The above data provides basis for device selection in the experimental prototype.

VI. EXPERIMENTAL VERIFICATION

The photo of the experimental platform is shown in Fig. 6. Inverter hardware in Fig. 6 provides the image of the prototype. The parameters and components of the prototype are shown in Table I.

Fig. 7(a) shows experimental waveforms of u_{Cr1} and i_{Ls1}, and it is seen that the experimental waveforms are similar

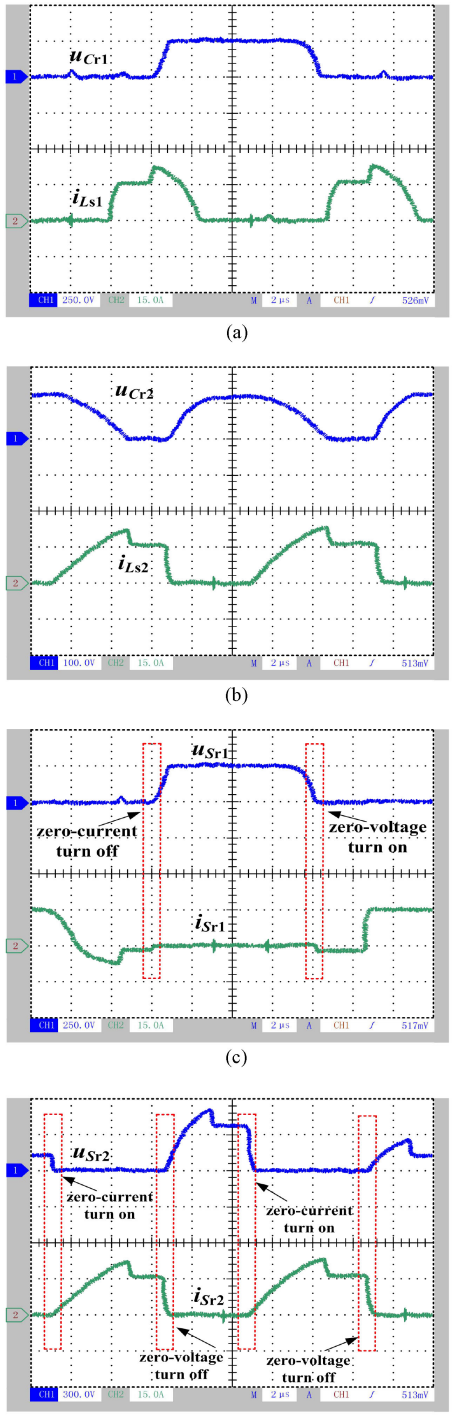

Fig. 7. Experimental waveforms. (a) Waveforms of the resonant current i_{Ls1} and the resonant voltage u_{Cr1} (scales: 250 V/div, 15 A/div, 2 μs/div). (b) Waveforms of the resonant current i_{Ls2} and the resonant voltage u_{Cr2} (scales: 100 V/div, 15A/div, 2 μs/div). (c) Waveforms of the terminal voltage u_{Sr1} and the current i_{Sr1} when the auxiliary switch S_{r1} is switched (scales: 250 V/div, 15 A/div, 2 μs/div). (d) Waveforms of the terminal voltage u_{Sr2} and the current i_{Sr2} when the auxiliary switch S_{r2} is switched (scales: 300 V/div, 15 A/div, 2 μs/div). (e) Waveforms of the terminal voltage u_{S1} and the current i_{S1} when the main switch S_1 is switched (at full load), (scales: 200 V/div, 5 A/div, 5 μs/div). (f) Waveforms of the terminal voltage u_{S1} and the current i_{S1} when the main switch S_1 is switched (at light load), (scales: 200 V/div, 5 A/div, 5 μs/div). (g) Waveforms of output line voltage u_{ab} of the inverter (scales: 100 V/div, 10 ms/div). (h) Waveforms of phase currents i_a, i_b, and i_c flowing through the three-phase load of the inverter (scales: 15 A/div, 4 ms/div).

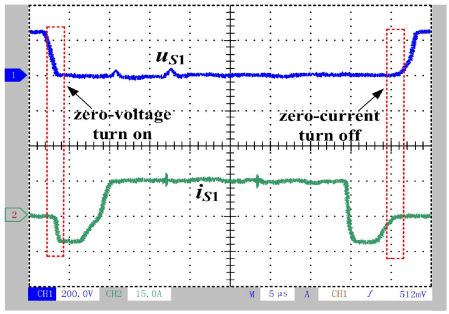

(e)

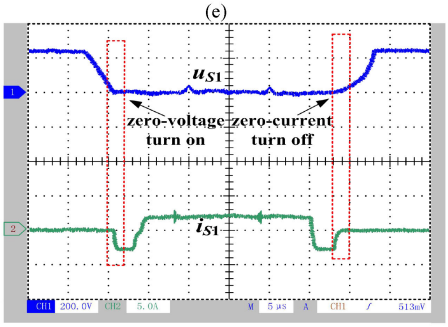

(f)

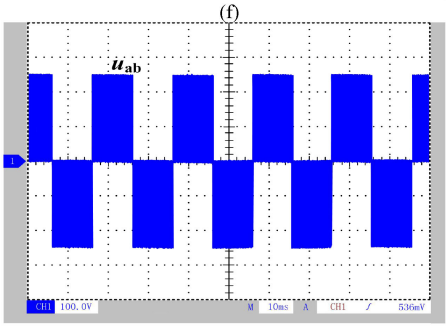

(g)

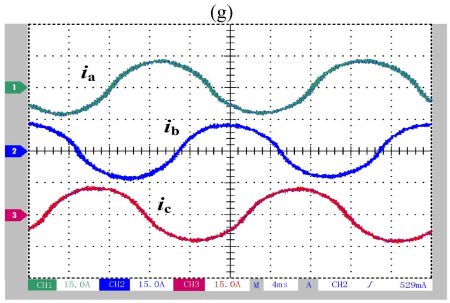

(h)

Fig. 7. Continued.

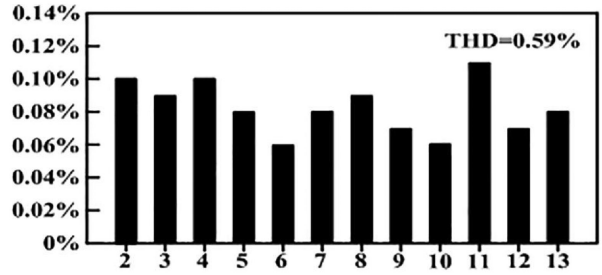

Fig. 8. Harmonic analysis of A-phase output current.

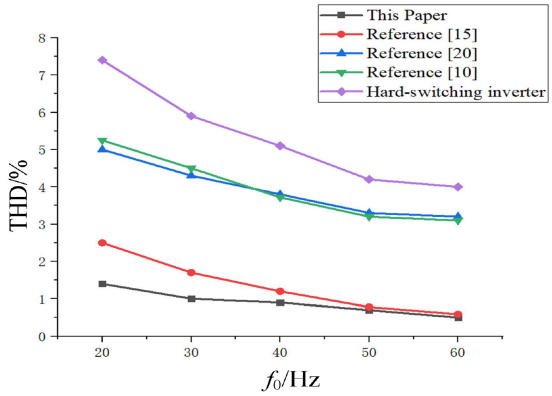

Fig. 9. Curve of the changing relationship between output frequency and THD of A-phase current in different inverters.

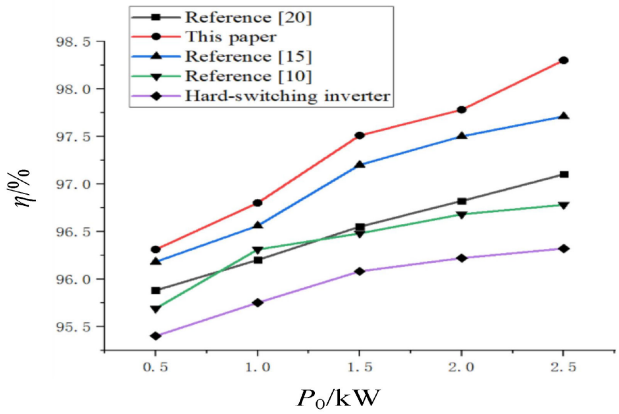

Fig. 10. Curve of the changing relationship between efficiency and output power.

to theoretical waveforms. Fig. 7(b) presents the experimental waveforms of u_{Cr2} and i_{Ls2}, and it is indicated that the experimental waveforms are similar to theoretical waveforms. As shown in Fig. 7(c), u_{Sr1} has reduced to zero before i_{Sr1} begins to change, and S_{r1} achieves zero-voltage turn-ON; i_{Sr1} has been zero before u_{Sr1} begins to change and S_{r1} achieves zero-current turn-OFF. As shown in Fig. 7(d), i_{Sr2} increases slowly and S_{r2} achieves zero-current turn-ON; u_{Sr2} increases slowly and S_{r2} achieves zero-voltage turn-OFF. As shown in Fig. 7(e) and (f), u_{S1} has been zero before i_{S1} changes and S_1 achieves zero-voltage turn-ON; i_{S1} has been zero before u_{S1} starts to change and S_1 achieves zero-current turn-OFF. Fig. 7(g) and (h) indicates the output line voltage u_{ab} and phase current waveforms of the inverter when output frequency is 50 Hz. As shown in Fig. 7(h), the sine degree of current waveform is well when output frequency is 50 Hz and the inverter runs well in the stable state.

Fig. 8 indicates the harmonic analysis of A-phase output current i_a of the presented inverter. As shown in Fig. 8, the total harmonic distortion (THD) of i_a is 0.59%. Fig. 9 displays the THD comparison of A-phase current. As shown in Fig. 9, the THD of A-phase current in the presented inverter in this article is lower than that in other resonant dc-link inverters, particularly with low output frequency.

Fig. 10 presents the measured efficiency. When the output power is 2.5 kW, the measured efficiency of the presented

TABLE II
NUMBER OF SWITCH AND SOFT SWITCHING ACTION AND STRESS

Number of switch	[10]		[15]		[20]		This paper	
Auxiliary switch	1		2		0		1	
Bus switch	0		1		1		1	
Diode	0		4		1		2	
Resonant capacitor	2		3		1		2	
Resonant inductor	1		2		2		2	
Soft switching	Turn-on	Turn-off	Turn-on	Turn-off	Turn-on	Turn-off	Turn-on	Turn-off
Main switch	ZVS	Pseudo ZVS	ZVS	Pseudo ZVS	ZVS	Pseudo ZVS	ZVS	ZCS
Auxiliary switch	ZVS	Pseudo ZVS	Pseudo ZCS	Pseudo ZVS	------	-----	Pseudo ZCS	Pseudo ZVS
Bus switch	------	-----	ZVS	Pseudo ZVS	Pseudo ZCS	Pseudo ZVS	ZVS	ZCS
Stress	Voltage	Current	Voltage	Current	Voltage	Current	Voltage	Current
Main switch	U_d+V_{Cc}	I_{omax} +I_{res}	U_d	I_{omax} +I_{res}	U_d	I_{omax} +I_{res}	U_d	I_{omax}
Auxiliary switch	U_d+V_{Cc}	I_{omax} +I_{res}	U_d	I_{omax} +I_{res}	------	-----	U_d+V_{Cc}	I_{omax} +I_{res}
Bus switch	------	-----	U_d	I_{omax}	U_d+U_d/n	I_{omax} +I_{res}	U_d	I_{omax}

NOTE: Body diodes are not included. U_d represents the dc supply voltage; V_{Cc} indicates the voltage of clamp capacitor; I_{omax} refers to the maximum load current; I_{res} stands for the additional resonant current; and n represents the turns ratio of coupled inductors.

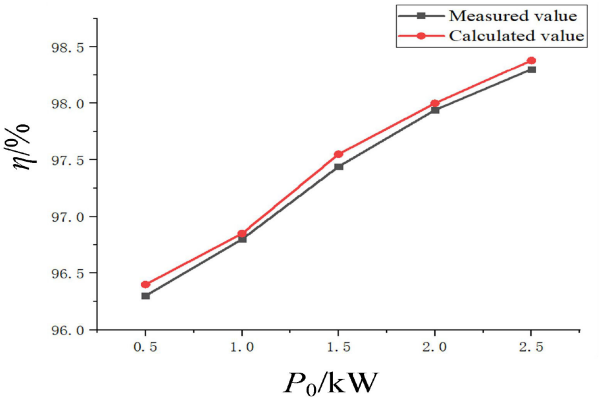

Fig. 11. Comparison between calculated efficiency and measured efficiency.

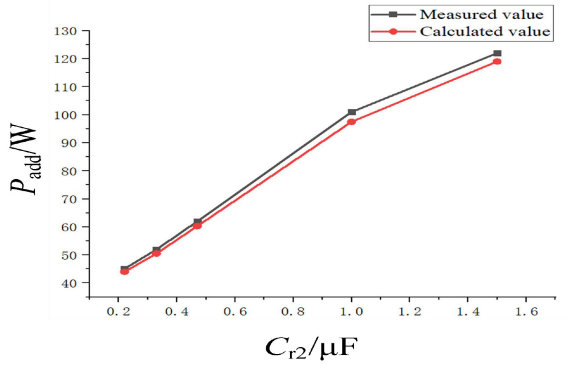

Fig. 12. Changing relation curve between C_{r2} and auxiliary resonant circuit loss.

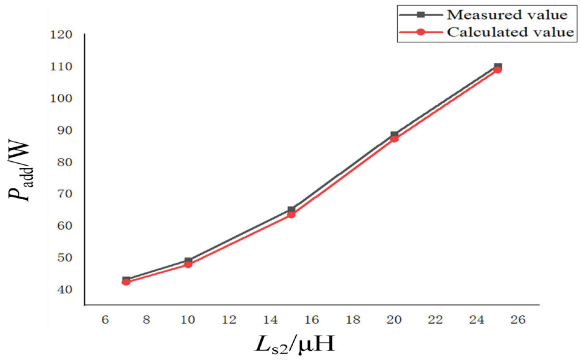

Fig. 13. Changing relation curve between L_{s2} and auxiliary resonant circuit loss.

inverter in this article is 98.3%, which is higher than the efficiency of the hard-switching inverter and soft-switching inverters in [10], [15], and [20]. It verifies the efficiency superiority of the inverter presented in this article.

Fig. 11 indicates the comparison between calculated efficiency and measured efficiency in the presented inverter. As shown in Fig. 11, the calculated efficiency is slightly higher than the measured efficiency, because the actual magnetic core loss and line loss are not included in the calculation. However, the changing curve of the calculated efficiency is very close to that of the measured efficiency, indicating that the mathematical model of power loss in the auxiliary resonant circuit is effective.

Figs. 12 and 13 present the changing curves of C_{r2}, L_{s2} and the auxiliary resonant circuit loss P_{add} when the output power is 2.5 kW. As can be seen from Figs. 12 and 13, when C_{r2} and L_{s2} increase, the measured value and theoretical value of P_{add} also increase, and the measured value is slightly greater than the calculated value, because the actual magnetic core loss and line loss are not included in the calculation. However, the changing curve of the calculated value is close to that of the measured value, suggesting that the theoretical analysis on the changing relationship between the auxiliary circuit loss and the resonant parameter is effective.

Fig. 14 shows the power loss distribution of soft-switching inverters in [10], [15], and [20], and the soft-switching inverter

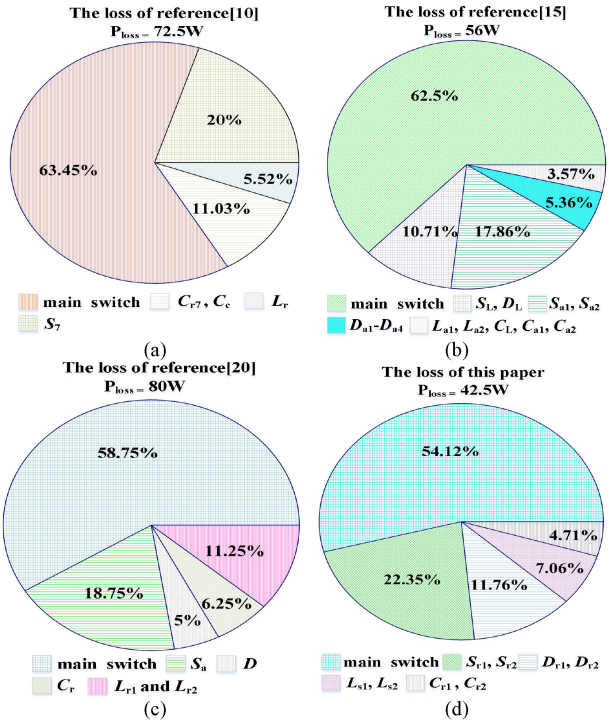

Fig. 14. Power loss distribution. (a) Reference [10]. (b) Reference [15]. (c) Reference [20]. (d) This article.

proposed in this article when the output power P_0 is 2.5 kW. The total loss of soft-switching inverter proposed in [10], [15], and [20] and this article are 72.5, 56, 80, and 42.5 W, respectively. It should be noted that the loss of coupled inductors in [20] and this article is, respectively, 9 and 3 W. The loss of the coupled inductors in the topology presented by this article is much lower than that in the similar topology presented in [20]. The location of the coupled inductors in this article is instrumental in reducing the power loss of the auxiliary circuit.

Table II demonstrates a comparison of the topology presented in [10], [15], and [20] and this article based on soft-switching type, the number of auxiliary devices and the maximum current and maximum voltage of the switching device. In Table II, elements that do not exist in each topology are marked with dashes. Compared with [10], the topology presented in this article can also diminish the maximum voltage and current of the main switch. It can be concluded from Table I that compared with [15], the topology presented in this article can diminish the current stress of the main switch and the number of auxiliary switches. Compared with [20], the topology presented in this article can diminish the maximum voltage and current of the bus switch.

VII. Conclusion

According to the existing problems of the inverters proposed in the related literature, this article puts forward a new auxiliary circuit structure to improve the property of the inverter, which is beneficial to the popularization and application of the soft-switching inverter. Based on theoretical analysis and experimental results, the following conclusions can be derived.

1) The main switching device and the bus switching device achieve zero-voltage turn-ON and zero-current turn-OFF. The auxiliary switching device achieves zero-current turn-ON and zero-voltage turn-OFF. MOSFET and IGBT can both be used as the main switching device and the bus switching device of the presented inverter, which widens the selection range of switching devices.
2) When the output power reaches 2.5 kW, the measured efficiency of the presented inverter is 98.3%, which verifies the efficiency superiority of the presented inverter in this article, compared with other soft-switching inverters. In the range of 0.5 to 2.5 kW, the calculated efficiency is close to the measured efficiency. The changing trends of the calculated efficiency and the measured efficiency are almost the same, which verifies high accuracy of theoretical calculation on the auxiliary circuit loss.
3) The sinusoidal degree of the output phase current is well and the auxiliary unit has no adverse influence on the stable work of the inverter. The THD of the output phase current is 0.59%, which is superior to other soft-switching inverters.
4) The duty cycle of the trigger pulse of the auxiliary switching device can be constant, which reduces the complexity of the control method in the auxiliary circuits.
5) The main switches of the inverter have no parallel resonant capacitors and coupled inductors are in the parallel branch of dc buses. The above distinguishing feature of the presented topology is instrumental in reducing the loss and optimizing the efficiency.

References

[1] E. Chu, X. Zhang, and L. Huang, "Research on a novel modulation strategy for double auxiliary resonant commutated pole soft-switching inverter with the shunt dead time," *IEEE Trans. Power Electron.*, vol. 31, no. 10, pp. 6855–6868, Oct. 2016.
[2] E. Chu, X. Zhang, Q. Sun, S. Li, H. Xiong, and X. Yang, "Three-phase double auxiliary resonant commutated pole inverter topology and analysis of its working principle," *IET Power Electron.*, vol. 9, no. 7, pp. 1536–1545, Jul. 2016.
[3] F. L. Tofoli and C. A. Gallo, "Analysis, design, and implementation of soft-switching cells applied to the single-phase full-bridge inverter," *IET Power Electron.*, vol. 9, no. 6, pp. 1249–1258, Jun. 2016.
[4] E. Chu, M. Wu, L. Huang, X. Hou, and H. Zhang, "Research on a novel modulation strategy for auxiliary resonant commutated pole inverter with the smallest loss in auxiliary commutation circuits," *IEEE Trans. Power Electron.*, vol. 29, no. 3, pp. 1103–1117, Mar. 2014.
[5] S. Pan, J. Pan, and Z. Tian, "A shifted SVPWM method to control DC-link resonant inverters and its FPGA realization," *IEEE Trans. Ind. Electron.*, vol. 59, no. 9, pp. 3383–3391, Sep. 2012.
[6] J. Chang and J. Hu, "Modular design of soft-switching circuits for two-level and three-level inverters," *IEEE Trans. Power Electron.*, vol. 21, no. 1, pp. 131–139, Jan. 2006.
[7] Q. Wang and Y. Wang, "Resonant DC link soft-switching inverter with low-loss auxiliary circuit," *Int. J. Electron.*, vol. 106, no. 10, pp. 1602–1615, Oct. 2019.
[8] S. Mandrek and P. J. Chrzan, "Quasi-resonant DC-link inverter with a reduced number of active elements," *IEEE Trans. Ind. Electron.*, vol. 54, no. 4, pp. 2088–2094, Apr. 2007.
[9] J. Shukla and B. G. Fernandes, "Three-phase soft-switched PWM Inverter for motor drive application," *IET Elect. Power Appl.*, vol. 1, no. 1, pp. 93–104, Jan. 2007.

[10] R. Li and D. Xu, "A zero-voltage switching three-phase inverter," *IEEE Trans. Power Electron.*, vol. 29, no. 3, pp. 1200–1210, Mar. 2014.
[11] C.-M. Wang, "A novel soft-switching single-phase AC-DC-AC converter using new ZVS-PWM strategy," *IEEE Trans. Power Electron.*, vol.22, no. 5, pp. 1941–1948, May 2007.
[12] C.-M. Wang, C. H., Lin, H. Y., Lin, and S. Y. Hsu, "Analysis, design and performance of a soft-switching single-phase inverter," *IET Power Electron*., vol. 7, no. 9, pp. 2412–2423, Sep. 2014.
[13] Z. Pan and F. Luo, "Transformer based resonant DC link inverter for brushless DC motor drive system," *IEEE Trans. Power Electron.*, vol. 20, no. 4, pp. 939–947, Jul. 2005.
[14] J. Kedarisetti and P. Mutschler, "A motor-friendly quasi-resonant DC-link inverter with lossless variable zero-voltage duration," *IEEE Trans. Power Electron.*, vol. 27, no. 5, pp. 2613–2622, May 2012.
[15] E. Chu, S. Li, H. Xie, J. Qiu, and H. Zhang, "RDCL three-phase inverter and load adaptive commutation control," *IET Power Electron.*, vol. 12, no. 3, pp. 505–514, Mar. 2019.
[16] B. Fazlali and E. Adib, "Quasi-resonant DC-link transformer-less structures for grid-connected PV systems," *Int. J. Elect. Power Energy Syst.*, vol. 103, no. 12, pp. 384–394, Dec. 2018.
[17] R. Gurunathan and A. K. S. Bhat, "Zero-voltage switching DC link single-phase pulsewidth-modulated voltage source inverter," *IEEE Trans. Power Electron.*, vol. 22, no. 5, pp. 1610–1618, Sep. 2007.
[18] Y. Chen*et al.*, "A ZVS grid-connected full-bridge inverter with a novel ZVS SPWM scheme," *IEEE Trans. Power Electron.*, vol. 31, no. 5, pp. 3626–3638, May 2016.
[19] M. R. Amini and H. Farzanehfard, "Quasi resonant DC link inverter with a simple auxiliary circuit," *J. Power Electron.*, vol. 11, no. 1, pp. 10–15, Jan. 2011.
[20] M. R. Amini and H. Farzanehfard, "Three-phase soft-switching inverter with minimum components," *IEEE Trans. Ind. Electron.*, vol. 58, no. 6, pp. 2258–2264, Jun. 2011.
[21] M. Mahdavi, M. R. Amini, A. Emrani, and H. Farzanehfard, "Soft switching three phase inverter with two auxiliary switches," *J. Power Electron.*, vol. 11, no. 6, pp. 787–792, Jun. 2011.

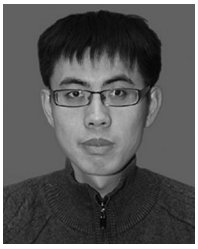

Qiang Wang received the B.S. degree in automation from Liaoning Technical University, Fuxin, China, in 2004, the M.S. degree in control theory and control engineering from Liaoning Technical University, Fuxin, China, in 2007, and the Ph.D. degree in control theory and control engineering from Northeastern University, Shenyang, China, in 2010.

Since 2010, he has been with the College of Information and Control Engineering, Liaoning Shihua University, Fushun, China, where he is currently an Assistant Professor. His research interests include high power dc/dc converter, inverter, and motor drive.

Guoxian Guo received the B.S. degree in electrical engineering and automation from Anyang Normal University, Anyang, China, in 2017. He is currently working toward the M.S. degree in electrical engineering with Liaoning Shihua University, Fushun, China.

His research interests include high-performance inverters and soft-switching techniques.

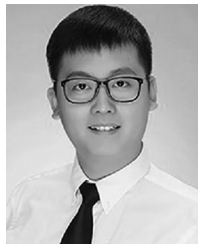

Youzheng Wang received the B.S. degree in electrical engineering and automation from Liaoning Shihua University, Funshun, China, in 2018. He is currently working toward the M.S. degree in electrical engineering with Liaoning Shihua University, Fushun, China.

His research interests include high-performance inverters and soft-switching techniques.

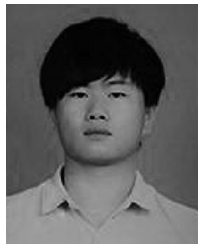

Jun Chen received the B.S. degree in electrical engineering and automation from Linyi University, Linyi, China, in 2018. He is currently working toward the M.S. degree in electrical engineering with Liaoning Shihua University, Fushun, China.

His research interests include high-performance inverters and soft-switching techniques.